Recruitment of Epac2A to Insulin Granule Docking Sites Regulates Priming for Exocytosis

Ida Alenkvist, Nikhil R. Gandasi, Sebastian Barg, and Anders Tengholm

Diabetes 2017;66:2610–2622 | https://doi.org/10.2337/db17-0050

Epac is a cAMP-activated guanine nucleotide exchange factor that mediates cAMP signaling in various types of cells, including β-cells, where it is involved in the control of insulin secretion. Upon activation, the protein redistributes to the plasma membrane, but the underlying molecular mechanisms and functional consequences are unclear. Using quantitative high-resolution microscopy, we found that cAMP elevation caused rapid binding of Epac2A to the β-cell plasma membrane, where it accumulated specifically at secretory granules and rendered them more prone to undergo exocytosis. cAMP-dependent membrane binding required the high-affinity cyclic nucleotide-binding (CNB) and Ras association domains, but not the disheveled–Egl-10–pleckstrin domain. Although the N-terminal low-affinity CNB domain (CNB-A) was dispensable for the translocation to the membrane, it was critical for directing Epac2A to the granule sites. Epac1, which lacks the CNB-A domain, was recruited to the plasma membrane but did not accumulate at granules. We conclude that Epac2A controls secretory granule release by binding to the exocytosis machinery, an effect that is enhanced by prior cAMP-dependent accumulation of the protein at the plasma membrane.

Control of protein localization is an important mechanism in signal transduction and regulation of cell function. The cAMP-activated guanine nucleotide exchange factors Epac1 and Epac2 mediate a variety of cAMP-regulated cellular processes, including neurotransmitter and hormone release, intracellular Ca^{2+} handling, cell adhesion, junction formation, cell proliferation, and gene transcription (1–7). They were recently found to undergo activity-dependent redistribution from the cytoplasm to the plasma membrane in different types of cells (8–10). The two proteins differ somewhat in tissue distribution and domain structure (1,7). Epac1 is relatively widely expressed, whereas Epac2 shows highest expression in the central nervous system, pancreas, and adrenals (1,11,12). Alternative promoter usage and splicing give rise to three isoforms of Epac2 (11,13). Both Epac1 and the Epac2 isoforms are multidomain proteins with an N-terminal regulatory region and a COOH-terminal catalytic region (14). The regulatory region consists of a low-affinity cyclic nucleotide-binding (CNB) domain (CNB-A; only present in the longest Epac2 splice version Epac2A [15]), a disheveled, Egl-10, and pleckstrin (DEP) domain, and a high-affinity CNB domain (CNB-B). The DEP domain is critical for the membrane binding of Epac1 (16), but its role in Epac2 is unclear, and the shortest isoform Epac2C lacks DEP domain. The catalytic region contains a Ras exchange motif, a Ras association (RA) domain, and a CDC25 homology domain. The latter domain catalyzes GTP/GDP exchange on the Rap family of small GTPases (1,12,17). In the absence of cAMP, Epac is inactive and maintained in a compact structure with the regulatory region blocking the catalytic domain (14). cAMP binding to the CNB domain(s) results in a conformational change that releases the autoinhibition and exposes the catalytic region (14,18,19). Only the high-affinity domain, CNB-B (K_d of 1.2 μmol/L [15]), seems important for catalytic regulation of Epac2 (18). The function of the CNB-A domain, with much lower affinity for cAMP (K_d 87 μmol/L [15]), is less clear, but it has been suggested to be involved in the subcellular targeting of Epac2 (11).

Epac2 has been found to positively regulate insulin secretion from pancreatic β-cells (4,20–22). We recently discovered that Epac2 activation results in translocation of the protein from the cytoplasm to the plasma membrane in insulin-secreting β-cells (10) in a process controlled by cAMP and Ca^{2+}, which in β-cells are key signals for exocytosis of insulin secretory granules (23). Glucose, the main

Department of Medical Cell Biology, Uppsala University Biomedical Centre, Uppsala, Sweden

Corresponding author: Anders Tengholm, anders.tengholm@mcb.uu.se.

Received 12 January 2017 and accepted 20 June 2017.

I.A. and N.R.G. contributed equally to this work.

physiological stimulator of insulin release, acts by increasing the concentrations of Ca^{2+} and cAMP in the β-cell cytoplasm, and the gut hormone glucagon-like peptide 1 (GLP-1) amplifies glucose-stimulated insulin secretion by stimulating cAMP production. Both glucose and GLP-1 were consequently found to induce translocation of Epac2 to the plasma membrane (10), but the detailed molecular targeting mechanisms and functional consequences are not clear. The cAMP-induced translocation of Epac2 requires intact high-affinity CNB-B and RA domains (10). However, the roles of the low-affinity CNB-A domain and the adjacent DEP domain remain unknown. In the current study, we have extended the analysis of the molecular mechanism underlying Epac2 membrane translocation and use a single-cell, real-time imaging approach to define the role of the different domains in the regulatory region of the protein. Furthermore, as Epac2 stimulates insulin secretion from β-cells, we investigated how Epac2 binding to the plasma membrane is related to insulin secretory granules and whether the translocation influences exocytosis. We found that Epac2A promotes granule priming and fusion by clustering at the exocytosis sites beneath the plasma membrane. This translocation involves two distinct localization mechanisms, one mediating membrane binding (CNB-B and RA domain) and another (CNB-A) directing Epac2A to components of the vesicle docking and fusion machinery.

RESEARCH DESIGN AND METHODS

Materials

3-Isobutyl-1-methylxanthine (IBMX), cAMP, GLP-1 (7–36 amide), forskolin, and poly-L-lysine were from Sigma-Aldrich (Stockholm, Sweden). Plasmids and adenovirus encoding mouse Epac2A fused to the fluorescent proteins EGFP or mCherry (GFP-Epac2A-wt and mCherry-Epac2A-wt) have been described (10), and a plasmid encoding yellow fluorescent protein–tagged Epac1 was a gift from Drs. J. Bos and H. Rehmann, University of Utrecht (Utrecht, the Netherlands). Point mutations were generated by site-directed mutagenesis, and domain deletions were created by PCR. Plasmids and adenovirus encoding fluorescence-tagged neuropeptide Y (NPY) to visualize secretory granules (24) and a cAMP-dependent protein kinase–based cAMP biosensor (25) have previously been reported.

Cell and Islet Culture

MIN6 β-cells (26) of passages 21–30 were cultured and transfected as described (10). Human islets were obtained from three normoglycemic (two male and one female; aged 67–73 years) and four cadaveric organ donors with type 2 diabetes (two male and two female; aged 55–59 years) via the Nordic Network for Clinical Islet Transplantation in Uppsala with approval from the Uppsala human ethics committee. The isolated islets were cultured up to 7 days as detailed in Tian et al. (27). For some experiments, the islets were dispersed into single cells and small clusters using cell dissociation buffer (Thermo Fisher Scientific) containing 10% trypsin. The cell suspension was added onto poly-L-lysine–coated coverslips and cultured overnight. The islets or cells were infected with adenovirus by 3- to 4-h incubation with 105 fluorescence-forming units per islet, followed by overnight culture before use.

Buffers

Most Epac translocation experiments were performed in experimental buffer containing 138 mmol NaCl, 4.8 mmol KCl, 1.2 mmol $MgCl_2$, 1.3 mmol $CaCl_2$, 3 mmol D-glucose, 25 mmol HEPES (pH 7.40), and 0.1% BSA. Coverslips with cells or islets were preincubated in this medium during 30–60 min, mounted in an open 50-μL chamber, and superfused with buffer at a rate of 0.2 mL/min. Where indicated, MIN6 cells were permeabilized with α-toxin as previously described (10). All of these experiments were performed at 37°C.

In granule localization experiments, the cells were maintained at 32°C in a solution containing 138 mmol NaCl, 5.6 mmol KCl, 1.2 mmol $MgCl_2$, 2.6 mmol $CaCl_2$, 3 mmol D-glucose, and 5 mmol HEPES (pH 7.4 with NaOH). In Figs. 7*A* and 8, exocytosis was evoked in medium containing 10 mmol/L D-glucose, 2 μmol/L forskolin, and 200 μmol/L diazoxide by computer-timed local application of high K^+ (75 mmol/L KCl equimolarly replacing NaCl) through a pressurized glass electrode. In Fig. 7*B*, exocytosis was stimulated by elevation of D-glucose to 20 mmol/L.

Microscopy

The subcellular localization of the fluorescent Epac constructs was assessed using spinning-disk (Andor Technology, Belfast, U.K.) (10) and point-scanning (Zeiss 780; Carl Zeiss, Oberkochen, Germany) confocal microscopes with 60×, numerical aperture 1.4 objectives (Nikon, Tokyo, Japan). Epac translocation, granule localization, and exocytosis were recorded with total internal reflection fluorescence (TIRF) microscopy. Most Epac2 experiments and the cAMP recordings were performed with an Eclipse Ti microscope (Nikon) with a TIRF illuminator and a 60×, numerical aperture 1.45 objective. Diode-pumped solid-state lasers (Cobolt, Stockholm, Sweden) provided excitation light at 491 (for EGFP) and 561 nm (mCherry). Fluorescence at 530-nm/50-nm half-bandwidth (EGFP) and 620-nm long-pass (mCherry) was detected with a back-illuminated EMCCD camera (iXON DU897; Andor Technology) controlled by MetaFluor software (Molecular Devices, Downingtown, PA). Images were acquired every 5 s. Granule localization and exocytosis experiments were made using a custom-built TIRF microscope based on an AxioObserver Z1 with a 100×/1.45 objective (Carl Zeiss) as described in Gandasi and Barg (28).

Image Analysis

Epac translocation was analyzed as changes in TIRF intensity over time in regions of interest corresponding to single cells. The signals were normalized to the prestimulatory level after background subtraction. All experiments

were repeated on at least two different cell preparations. The data are expressed as means ± SE or as scatter plots with highlighted median values. Two-tailed Student *t* test or Wilcoxon signed-rank test was used to assess statistical differences.

Colocalization of Epac with secretory granules was quantified essentially as described (29). In brief, an algorithm implemented in MetaMorph read the average fluorescence in a central circle (c) of three-pixel (0.5 μm) diameter, a surrounding annulus (a) with a five-pixel outer diameter, and a cell-free background area (bg). The specific on-granule fluorescence was defined as $\Delta F = c - a$. To obtain off-granule fluorescence, S, the annulus value was background-corrected ($S = a - bg$). $\Delta F/S$ is a measure of the degree of binding to the granule location (28). Positive values indicate enrichment and negative values exclusion from the granule site.

In Figs. 4–6, the $\Delta F/S$ value for each cell represents an average from a time-series of 50 consecutive frames. In Fig. 7, $\Delta F/S$ was calculated for every frame, and only cells with intensity level (cell − background) >200 (16-bit digitization) were included. Note that ΔF is given as per-pixel average for the entire 0.5-μm circle, and $\Delta F/S$ values are therefore seemingly small. Assuming a cluster size of 50 nm, $\Delta F/S = 0.1$ corresponds to at least 20-fold enrichment in the cluster beneath a granule. Single-granule exocytosis events were detected manually as a sudden (less than three frames) drop in fluorescence.

RESULTS

Epac2A Binding to the Plasma Membrane Does Not Require the DEP or CNB-A Domains

To determine the mechanisms underlying Epac2A binding to the plasma membrane, fluorescent protein–tagged deletion mutants lacking either the low-affinity cAMP-binding CNB-A domain (mCherry-Epac2A-ΔCNB-A) or the DEP domain (mCherry-Epac2A-ΔDEP) were expressed together with wild-type Epac2A (GFP-Epac2A-wt) in MIN6 cells (Fig. 1*A*). As previously reported (10), cAMP elevation by the phosphodiesterase inhibitor IBMX (100 μmol/L) induced translocation of wild-type Epac2A, recorded in TIRF microscopy as an increase of fluorescence in the cell footprint area (Fig. 1*B*). Quantification of the IBMX responses showed that the translocation of the ΔCNB-A mutant was more pronounced than wild-type and that of ΔDEP impaired (Fig. 1*C* and *D*). Control experiments showed nearly identical translocation of coexpressed GFP- and mCherry-tagged Epac2A-wt, indicating that translocation responses can be quantitatively compared between different Epac2 constructs (Fig. 1*E* and *F*). The reduced translocation of the ΔDEP mutant may be explained by increased prestimulatory membrane association, as evaluated by confocal imaging of wild-type and mutant Epac2A (Fig. 1*G*). Both constructs showed a fairly homogenous cytoplasmic distribution. The relative membrane/cytoplasm intensity for ΔDEP was 0.89 ± 0.04 vs. 0.73 ± 0.04 for coexpressed wild-type Epac2A ($P < 0.01$; $n = 14$ cells and 4 experiments) and 0.72 ± 0.03 for ΔCNB-A vs. 0.72 ± 0.05 for wild-type ($n = 12$ cells and 4 experiments) in unstimulated cells.

The CNB-A Domain Limits Epac2A Translocation at Low and Enhances Translocation at High cAMP Concentrations

The cAMP dependence of Epac2A translocation was analyzed in permeabilized MIN6 cells. Superfusion of increasing cAMP concentrations resulted in dose-dependent membrane translocation of Epac2A-wt with half-maximal translocation at 21 μmol/L and maximal effect at ∼100 μmol/L (Fig. 2*A–C*). The ΔCNB-A mutant showed more pronounced translocation than wild-type at 1–10 μmol/L cAMP, but the maximal translocation amplitude was smaller and obtained already at 30 μmol/L cAMP (Fig. 2*D* and *F*). The DEP-deficient mutant showed very modest translocation, reaching maximum at 10 μmol/L cAMP (Fig. 2*E* and *F*). The averaged data in Fig. 2*F* show that the cAMP dependence of the translocation was left-shifted in the mutants with half-maximal effect obtained at 5.6 ± 1.2 and 1.7 ± 1.9 μmol/L for ΔCNB-A and ΔDEP, respectively.

GLP-1 Promotes cAMP-Dependent Epac2A Translocation

We next investigated how a physiological stimulus of cAMP formation in β-cells, the insulinotropic hormone GLP-1, influenced Epac2A localization. At 1 nmol/L, GLP-1 evoked a prompt rise of the cAMP concentration, which was associated with translocation of Epac2A to the plasma membrane (Fig. 3*A*). GLP-1– and cAMP-induced Epac2A translocation was not restricted to the cell line, but also observed in human pancreatic islet cells (Fig. 3*B*). The molecular determinants of the translocation were further characterized in MIN6 cells. Like IBMX, GLP-1 stimulated more pronounced translocation of the ΔCNB-A mutant than of Epac2-wt (Fig. 3*C*). The translocation response was amplified also by a point mutation that prevents cAMP binding to the CNB-A domain (G114E [2]) (Fig. 3*D*). In contrast, mCherry-Epac2A-ΔDEP showed poor translocation in response to GLP-1 (Fig. 3*E*). Consistent with previous observations (10), a point mutation preventing cAMP binding of the CNB-B domain (G422D [2]), or one in the RA domain preventing binding to Ras-GTP (K684E [30]), strongly suppressed GLP-1–induced Epac2A translocation (Fig. 3*F–H*).

Epac2A Accumulates at Docked Secretory Granules

To analyze the distribution of Epac2 in relation to the localization of near-membrane insulin granules, the cells were cotransfected with NPY-EGFP as granule marker and mCherry-labeled Epac2 versions and imaged with TIRF microscopy. In unstimulated cells exposed to 3 mmol/L glucose, mCherry-Epac2A-wt distributed diffusely throughout the footprint area of the cell with slight preference for granules ($\Delta F/S = 0.010 \pm 0.003$ vs. 0 for random locations;

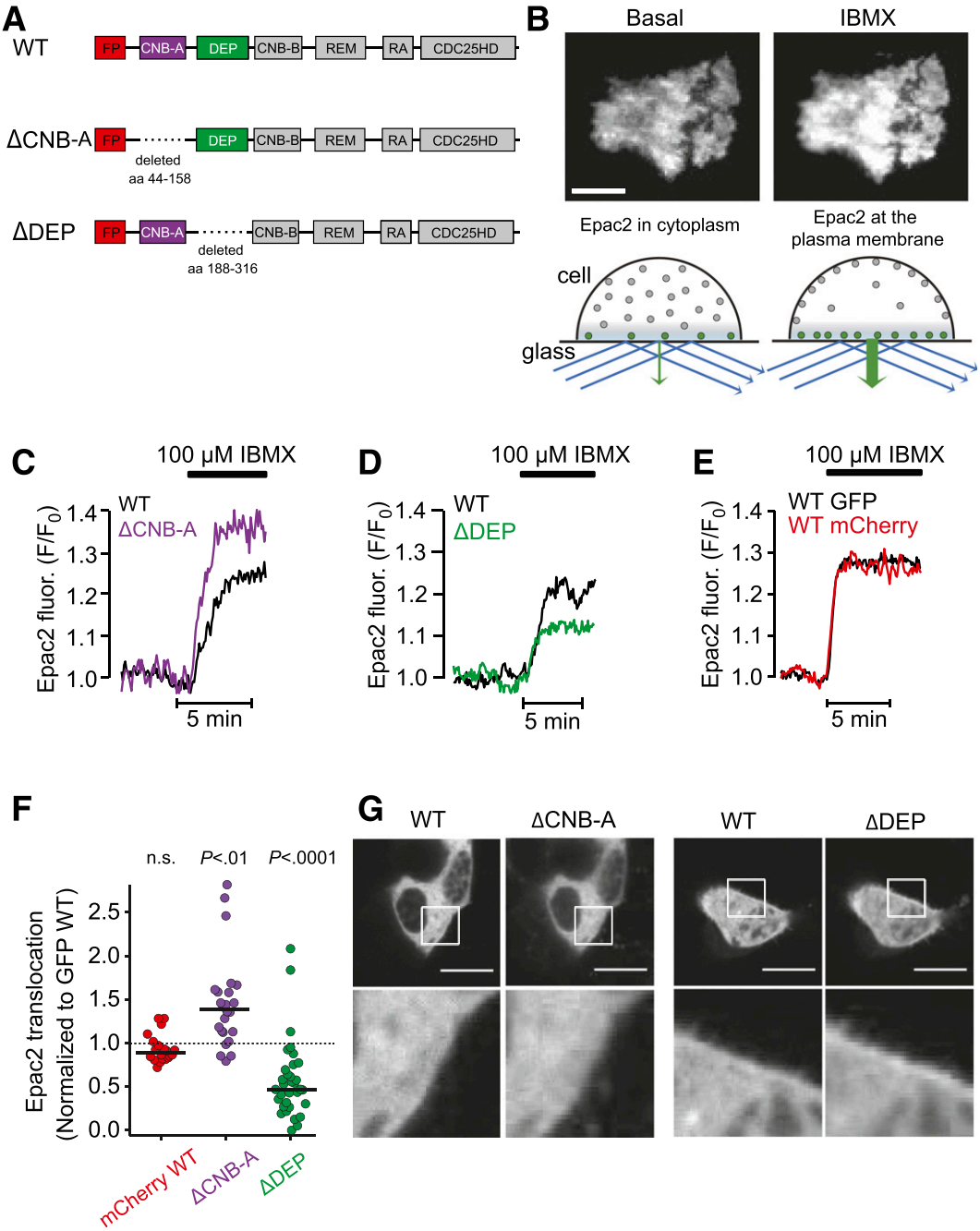

Figure 1—Epac2A translocation to the plasma membrane can occur without involvement of the DEP and CNB-A domains. *A*: Fluorescent protein fusion constructs with full-length wild-type Epac2A (WT); Epac2A lacking amino acids 44–158, corresponding to the CNB-A domain (ΔCNB-A); and 188–316, corresponding to the DEP domain (ΔDEP). CDC25HD, Cdc25 homology domain; FP, green fluorescent protein or mCherry; REM, Ras exchange motif. *B*: TIRF images of GFP-Epac2A-wt in MIN6 cells before and after stimulation with 100 μmol/L IBMX. Scale bar, 10 μm. The schematic drawing shows how plasma membrane association of the construct results in increased TIRF intensity. Blue arrows indicate incident laser excitation light and green arrows fluorescent light. Time-lapse TIRF intensity recordings from single MIN6 cells coexpressing GFP-Epac2A-wt and mCherry-Epac2A-ΔCNB-A (*C*), mCherry-Epac2A-ΔDEP (*D*), or mCherry-Epac2A-wt (*E*) during stimulation with IBMX. *F*: Scatter plots for the amplitude of the IBMX-induced translocation normalized to that of GFP-Epac2A-wt and with highlighted median values. $n = 20$ cells from 4 experiments for mCherry wt, 24 cells from 7 experiments for ΔCNB-A, and 33 cells from 6 experiments for ΔDEP. *P* values refer to differences from the GFP wt control indicated by the dashed line (Wilcoxon signed-rank test). *G*: Confocal images of MIN6 cells coexpressing GFP-Epac2A-wt and either mCherry-Epac2A-ΔCNB-A (representative for 12 cells in 4 experiments) or mCherry-Epac2A-ΔDEP (representative for 14 cells in 4 experiments). Scale bars, 10 μm. The bottom panel shows enlargements of the areas highlighted by the squares in the top panel.

$P < 0.001$) (Fig. 4). After elevation of cAMP with 2 μmol/L of the adenylyl cyclase activator forskolin, ~40% of the cells showed apparent clustering of Epac2A at the sites of docked granules. The extent of clustering was related to expression level and most pronounced in cells with weak mCherry-Epac2A fluorescence (data not shown). Average ΔF/S for

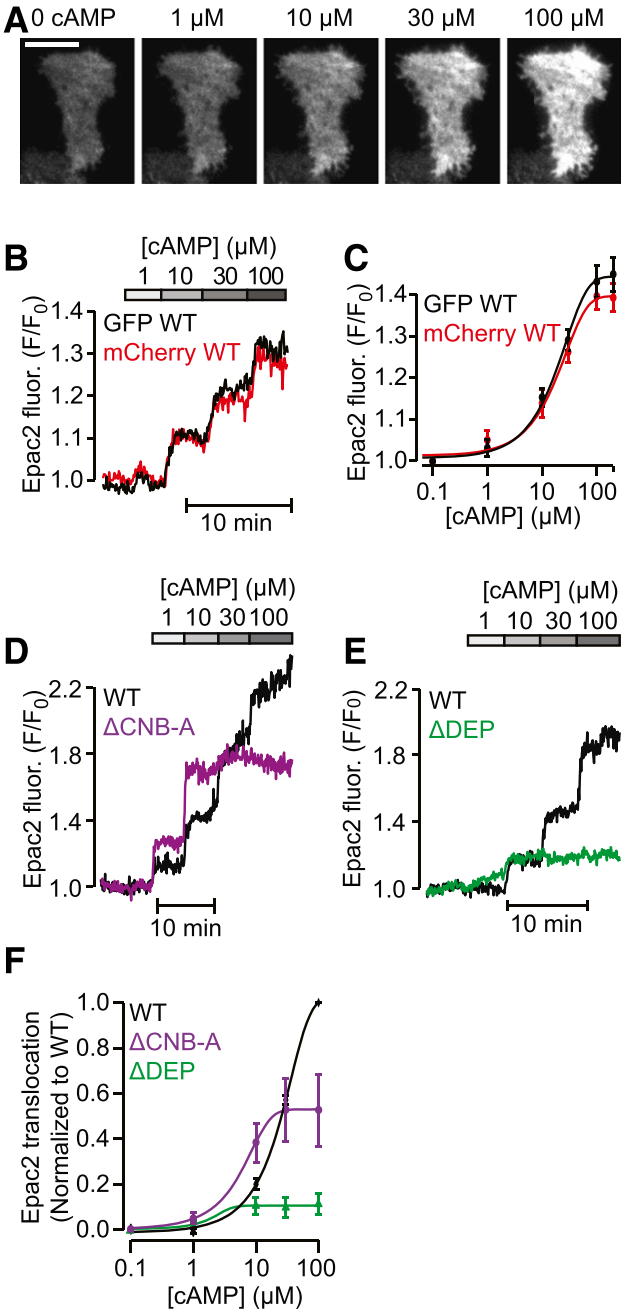

Figure 2—Dual effects of the CNB-A domain on cAMP-dependent Epac2A translocation. *A*: TIRF image time series of an α-toxin–permeabilized individual MIN6 cell expressing mCherry-Epac2A-wt during exposure to increasing concentrations of cAMP. Scale bar, 10 μm. *B*: Time-lapse TIRF intensity recording from a single permeabilized MIN6 cell coexpressing GFP- and mCherry-tagged Epac2A-wt and exposed to varying concentrations of cAMP. *C*: Means ± SE for the steady-state fluorescence intensity at different cAMP concentrations. $n = 5$ cells from five experiments. The lines represent sigmoidal fits to the data. TIRF recordings from permeabilized cells coexpressing GFP-Epac2A-wt and either mCherry-Epac2A-ΔCNB-A (*D*) or mCherry-Epac2A-ΔDEP (*E*) during exposure to different cAMP concentrations. *F*: Dose dependence of the cAMP-induced Epac2A translocation normalized to the effect of 100 μmol/L cAMP on GFP-Epac2A-wt. Means ± SE. The lines are sigmoidal fits to the data. $n = 26$ cells from 5 experiments for wt, 12 cells from 4 experiments for ΔCNB-A, and 14 cells from 5 experiments for ΔDEP.

all cells increased sixfold in the presence of forskolin ($P < 0.001$) (Fig. 4).

Epac2A Targeting to Granule Sites Depends on CNB-A but Not the DEP Domain

Forskolin failed to induce clustering of Epac2A with point mutations in the high-affinity cAMP-binding CNB-B domain (G422D) and the RA domain (K684E) (Fig. 4). Granule-associated clusters were also absent with ΔCNB-A and the mutant with cAMP binding–deficient CNB-A domain (G114E). In contrast, the ΔDEP mutant clustered to the same extent as the forskolin-treated wild-type ($P < 0.001$ vs. wild-type control), irrespective of forskolin (Fig. 4). These findings could not be explained by systematic differences in expression of the various constructs (data not shown). Instead, the data demonstrate that the DEP domain is not required for the targeting of Epac2A to granule sites and that the CNB-A domain is dispensable for membrane recruitment, but important for the specific interaction with the granule docking sites.

Epac2A clustering was also induced by GLP-1 (10 nmol/L) in both MIN6 cells and human islet cells (Fig. 5*A*). This clustering was reduced in cells from donors with type 2 diabetes (Fig. 5*A*). Although not statistically significant, the granule clustering (ΔF/*S*) tended to correlate inversely with HbA_{1c} for all human donors ($R^2 = 0.86$) (Fig. 5*B*). Consistent with a role for the CNB-A domain for localization of Epac2A to granule sites, expression of the isolated CNB-A domain (including the preceding N-terminal 42 amino acid residues) demonstrated significant colocalization with vesicles (ΔF/*S* more than fivefold over random locations; $P = 0.0024$) (Fig. 6*A*). GLP-1 stimulation tended to reduce this clustering, possibly because of competition from endogenous Epac2A. We also tested if glucose induced Epac2A clustering. Indeed, cells exposed to 20 mmol/L glucose showed significantly higher ΔF/*S* than those maintained at 3 mmol/L (Fig. 6*B*).

Epac1 Translocates to the Plasma Membrane but Fails to Cluster at Granule Docking Sites

To further investigate the mechanisms underlying Epac2A binding to granule sites, we investigated the closely related Epac1, which lacks an N-terminal CNB domain and therefore resembles the ΔCNB-A mutant of Epac2A. Yellow fluorescent protein–tagged Epac1 translocated to the plasma membrane in response to cAMP elevation with IBMX and forskolin (Fig. 6*C*). Comparison of coexpressed Epac1 and Epac2A in permeabilized cells showed lower maximal translocation amplitude for Epac1 (Fig. 6*D* and *E*). Moreover, the dose response was left-shifted with half-maximal translocation at 7.7 μmol/L cAMP for Epac1 vs. 17 μmol/L for Epac2A and maximal translocation at ~30 and 100 μmol/L, respectively (Fig. 6*E*). Analyzing the protein distribution in the plasma membrane, Epac1 showed only a weak, albeit significant ($P < 0.005$), tendency to cluster near granule docking sites in response to forskolin (Fig. 6*F* and *G*).

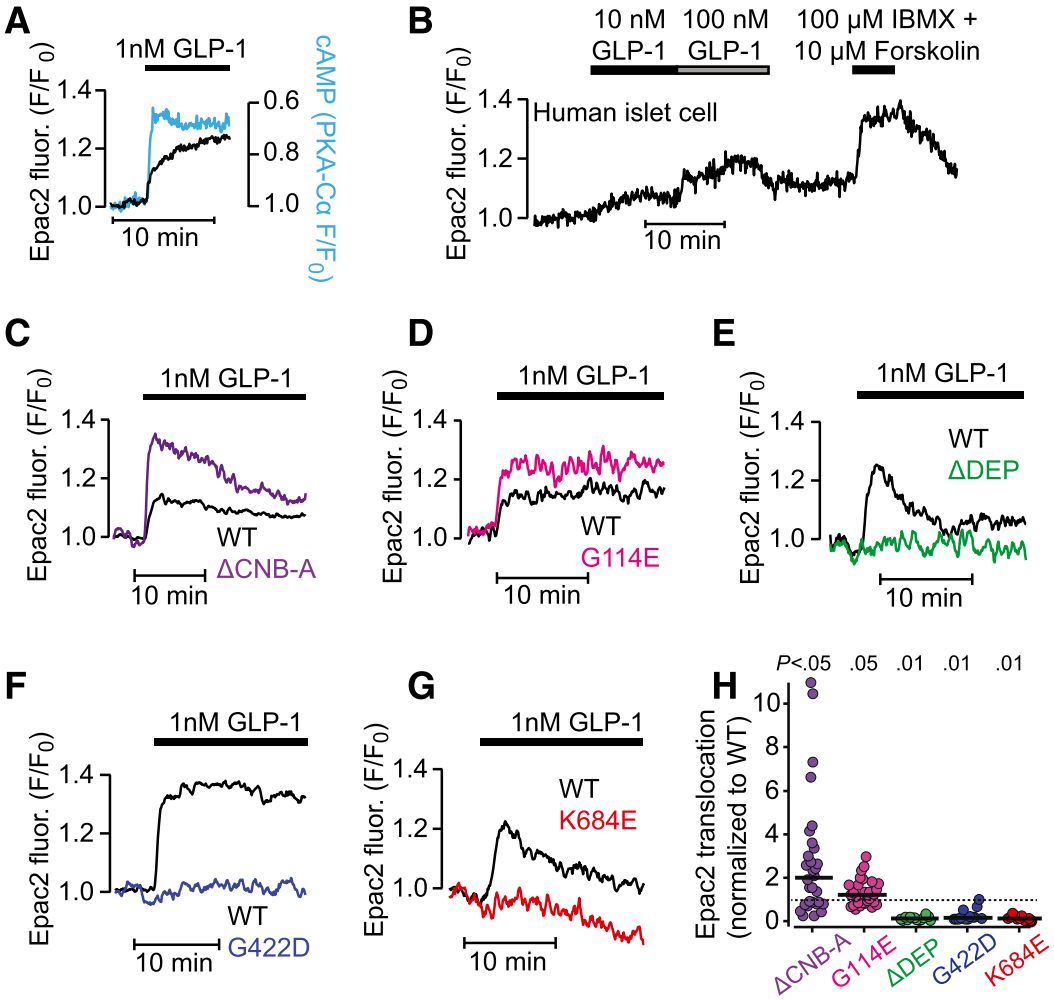

Figure 3—GLP-1 triggers cAMP-dependent Epac2A translocation in β-cells. *A*: Simultaneous TIRF recording of submembrane cAMP concentration (blue trace) and Epac2A membrane association (black trace) in a single MIN6 cell stimulated with 1 nmol/L GLP-1 in the presence of 3 mmol/L glucose. *B*: TIRF intensity recording of mCherry-Epac2A-wt in a single cell within an intact human pancreatic islet exposed to 10–100 nmol/L GLP-1 and a combination of 100 μmol/L IBMX and 10 μmol/L forskolin. TIRF recordings from single cells coexpressing GFP-Epac2A-wt and mCherry-Epac2A-ΔCNB-A (*C*), mCherry-Epac2A-G114E (*D*), mCherry-Epac2A-ΔDEP (*E*), mCherry-Epac2A-G422D (*F*), or mCherry-Epac2A-K684E (*G*) during stimulation with GLP-1. *H*: Scatter plots of the GLP-1–induced Epac2A translocation amplitude normalized to that of GFP-Epac2A-wt and with the median values highlighted. ΔCNB-A, n = 30 cells from 7 experiments; G114E, n = 29 cells from 6 experiments; ΔDEP, n = 14 cells from 4 experiments; G422D, n = 13 cells from 3 experiments; and K684E, n = 11 cells from 3 experiments. P values refer to differences from the wt control indicated by the dashed line (Wilcoxon signed-rank test).

Binding of Epac2A to the Exocytosis Machinery Promotes Granule Priming and Exocytosis

To test how Epac2A association with granule docking sites at the plasma membrane affects exocytosis, the cells were stimulated by depolarization with 75 mmol/L K^+ in the presence of 10 mmol/L glucose, 200 μmol/L diazoxide, and 2 μmol/L forskolin. Exocytotic events, seen as rapid disappearance of NPY-GFP, were observed immediately after onset of the stimulation (Fig. 7*A*). The analysis was restricted to cells that showed clustered Epac2A fluorescence. All granules undergoing exocytosis were selected and matched with other granules in the same cell that failed to respond to the stimulation. The former group corresponds to primed granules, whereas the latter are merely docked (28). Fluorescence from granules undergoing exocytosis decayed to zero, whereas it remained constant in time-matched controls (Fig. 7*A*). The granule-associated Epac2A signal, quantified as ΔF/S, was significantly higher in exocytosing granules compared with the failures ($P < 0.001$) (Fig. 7*A*). We also analyzed glucose-induced exocytosis events. Granules undergoing exocytosis in cells stimulated with 20 mmol/L glucose showed less Epac2A clustering than with forskolin treatment, but significantly more than granules failing to fuse ($P < 0.001$) (Fig. 7*B*). The data indicate that recruitment of Epac2A to granules correlates with their priming.

Next, we investigated how Epac2A mutants with different granule localization influenced insulin secretion by quantifying the number of exocytosis events after stimulation with high K^+. Figure 8*A* shows that forskolin amplified

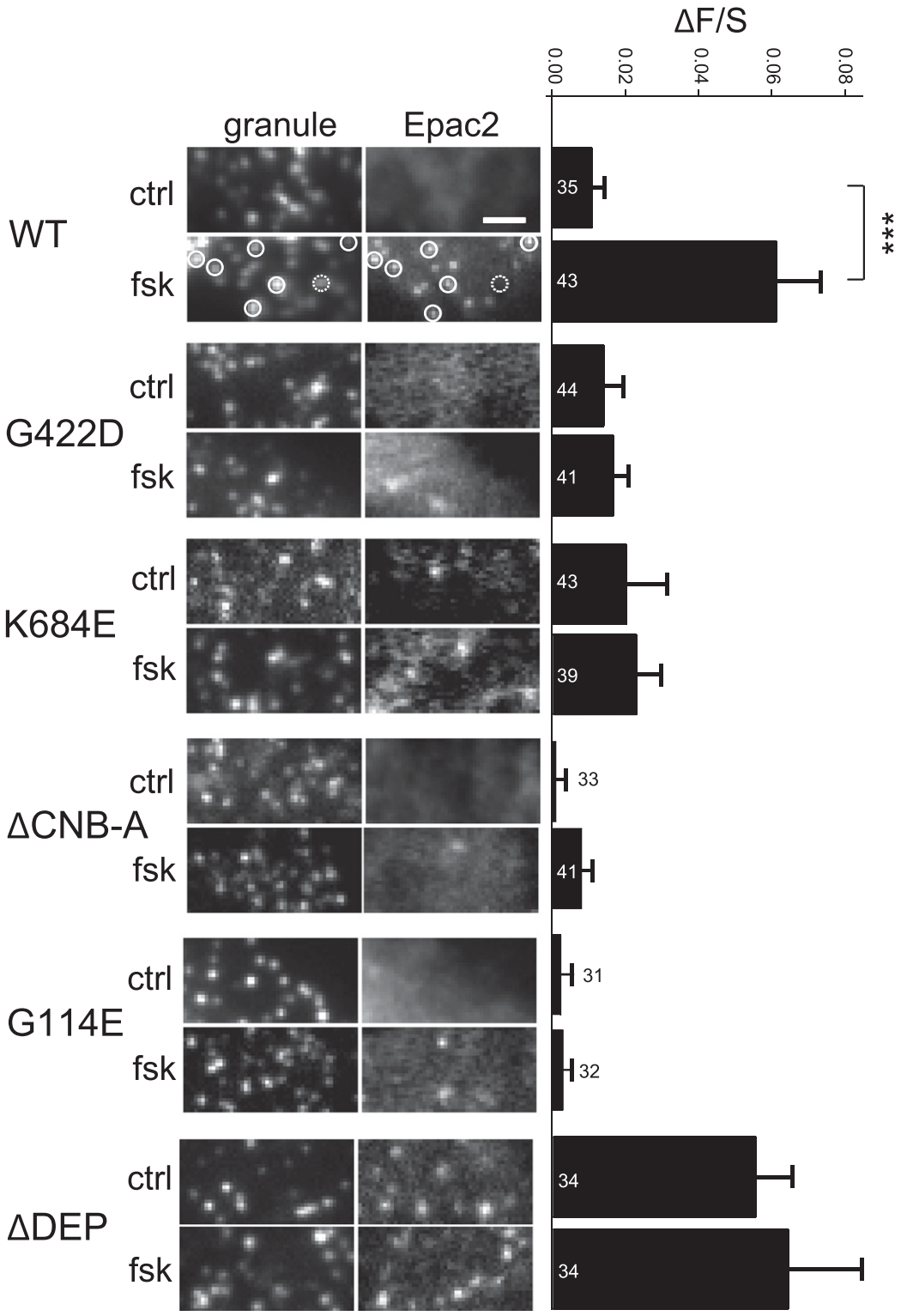

Figure 4—Epac2A accumulates at docked secretory granules. TIRF images of MIN6-cells coexpressing NPY-mEGFP (granule) and mCherry-tagged versions of Epac2 under basal conditions (ctrl) and after exposure to 2 μmol/L forskolin (fsk). Image pairs of the two color channels were acquired sequentially, first with cells exposed to 561 nm (1 mW) at 50 × 20-ms exposure and averaged, immediately followed by exposure to 491 nm (0.5 mW) for 100 ms. After fsk stimulation, many granules colocalized with Epac2 clusters, as illustrated with solid circles in the wild-type image. The dashed circle shows an example of a granule without an Epac2 cluster. The accumulation of Epac2 at granule sites was quantified as ΔF/S, as described in Research Design and Methods. Positive values indicate Epac2 accumulation at the granules, whereas ΔF/S = 0 for random distributions. Bars show means ± SE. Number of cells from at least three experiments are stated at each bar. ΔCNB-A, mCherry-Epac2A-ΔCNB-A; ΔDEP, mCherry-Epac2A-ΔDEP; G114E, mCherry-Epac2A-G114E; G422D, mCherry-Epac2A-G422D; K684E, mCherry-Epac2A-K684E; WT, mCherry-Epac2A-wt. ***$P < 0.001$ for difference from wt control. Scale bar, 2 μm.

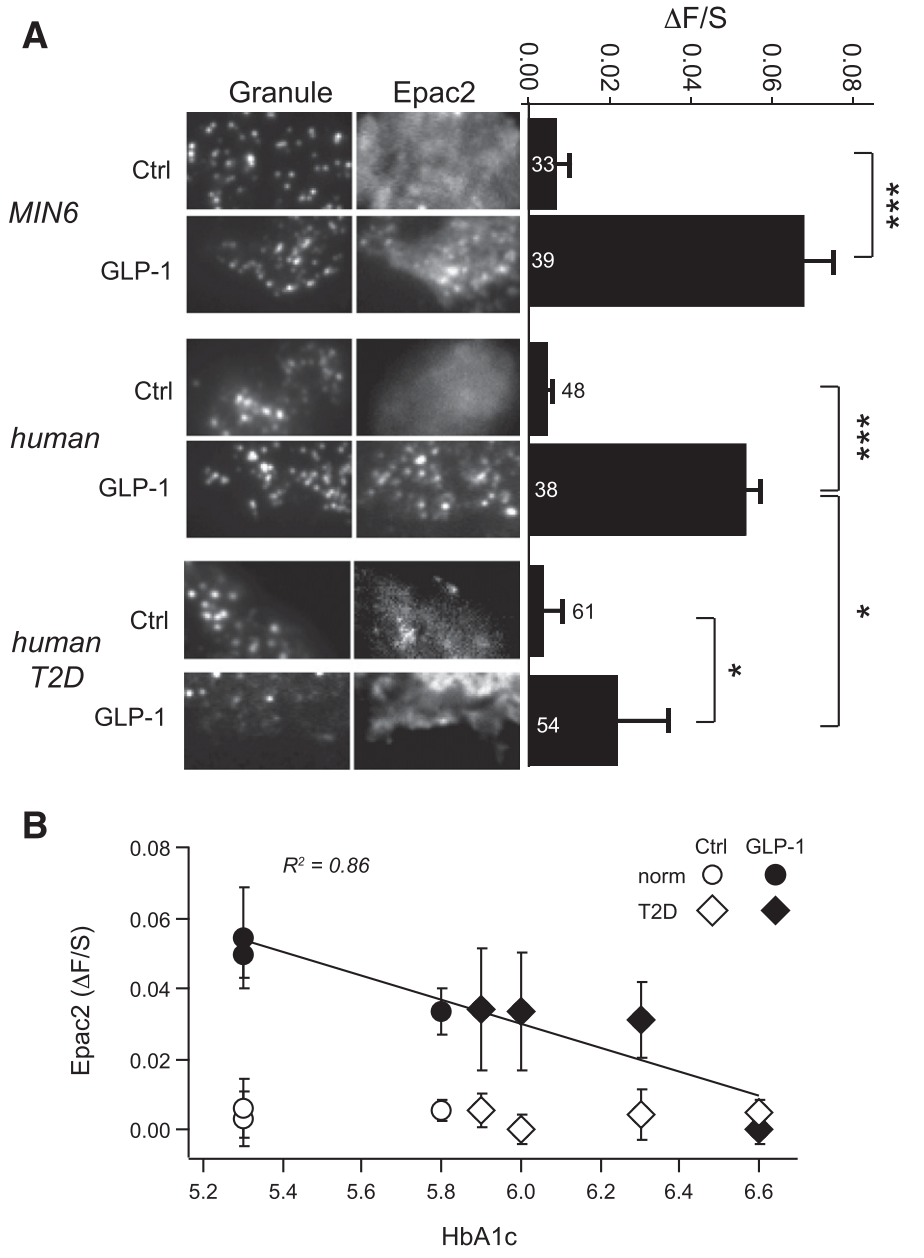

Figure 5—GLP-1 induces clustering of Epac2A at docked secretory granules. *A*: TIRF images of MIN6 cells and human islet cells (from normoglycemic donors or donors with type 2 diabetes) coexpressing NPY-mEGFP (granule) and mCherry-Epac2A-wt under basal conditions (Ctrl) and after exposure to 10 nmol/L GLP-1. The bar graphs show means ± SE for the accumulation of Epac2 at granule docking sites quantified as ΔF/S. Number of cells from at least three experiments is shown for each bar. GLP-1 induces Epac2 clustering in both MIN6 cells and single human pancreatic islet cells, and this aggregation is reduced in cells from donors with diabetes. *B*: Epac2 granule accumulation (ΔF/S) as a function of HbA_{1c} in all human donors under control conditions (open symbols) and in the presence of GLP-1 (closed symbols). Values from normoglycemic donors (norm) are shown as circles and those from donors with type 2 diabetes (T2D) as diamonds. The linear regression regards data with GLP-1, but the correlation is not significant. *$P < 0.05$; ***$P < 0.001$ for difference.

secretion several-fold in cells expressing mCherry-Epac2A-wt. The response was significantly ($P < 0.001$) attenuated in cells expressing the translocation-incapable G422D mutant, the ΔCNB-A mutant, unable to accumulate at granules, and the ΔDEP mutant, which constitutively localizes to the granule sites (Fig. 8*B*). These findings show that Epac2A localization to the docking sites is necessary, but not sufficient, to promote exocytosis.

DISCUSSION

The Epac proteins are widely expressed cAMP sensors, which recently have been found to translocate from the cytoplasm to the plasma membrane upon activation (8–10). In the current study, we investigated the mechanisms and functional relevance of this spatiotemporal regulation in β-cells and found that Epac2A clusters at secretory vesicle docking sites. This distribution pattern is achieved by a dual

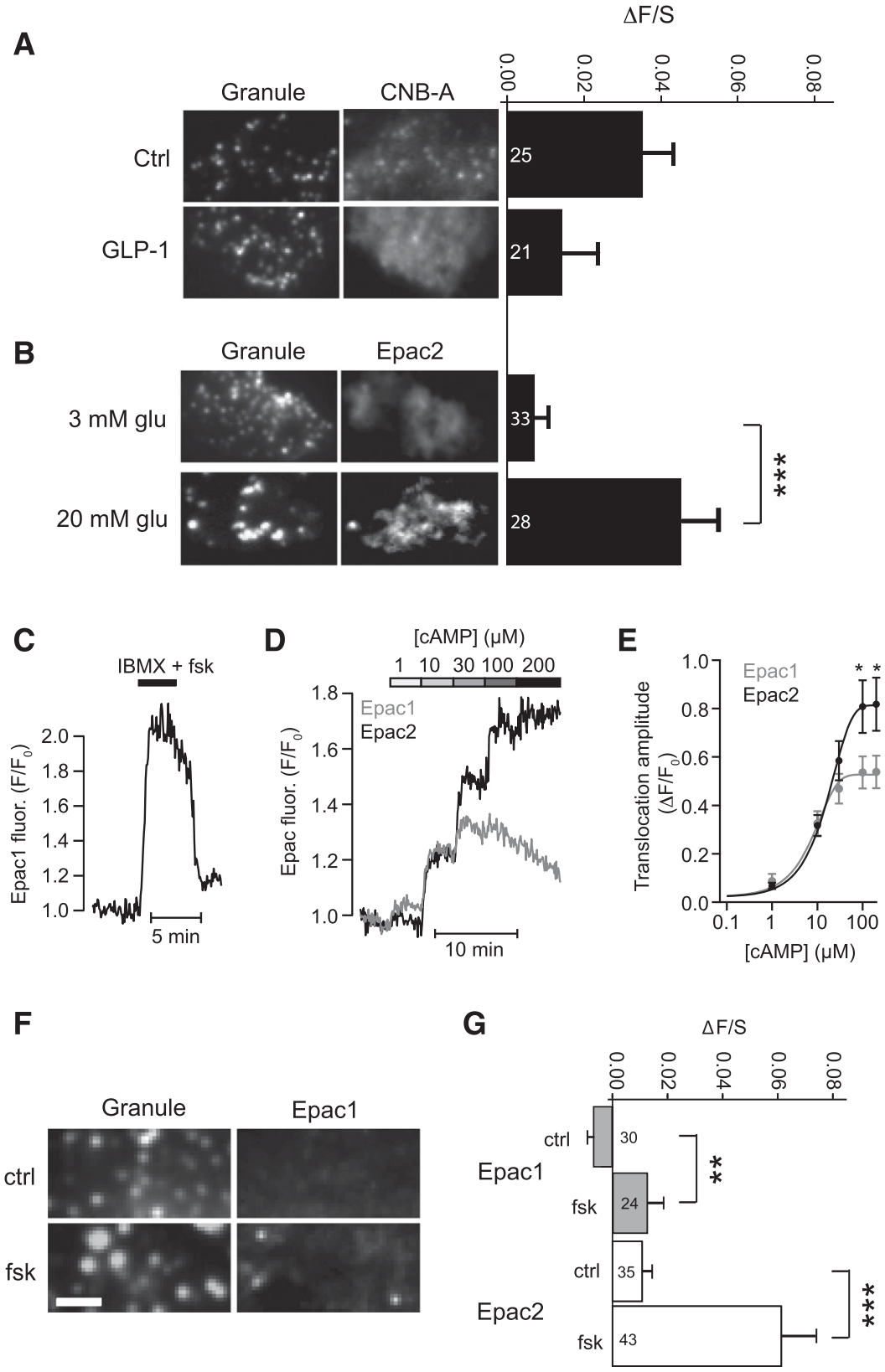

Figure 6—Comparison of Epac2 and Epac1 translocation and granule-associated clustering. *A*: TIRF images of MIN6 cells coexpressing NPY-mEGFP (granule) and mCherry-tagged isolated CNB-A domain under basal conditions (Ctrl) and after exposure to 10 nmol/L GLP-1. The bar graphs show means ± SE for the accumulation of Epac2 at granule docking sites quantified as ΔF/S. Number of cells from at least three experiments is shown for each bar. The CNB-A domain localizes to docked secretory granules in unstimulated cells. *B*: Similar analysis of cells expressing NPY-mEGFP (granule) and wild-type Epac2A during exposure to 3 and 20 mmol/L glucose. Glucose promotes granule accumulation of Epac2A. ***$P < 0.001$ for difference. *C*: TIRF intensity recording of GFP-Epac1 in a single MIN6-cell exposed to 100 μmol/L IBMX and

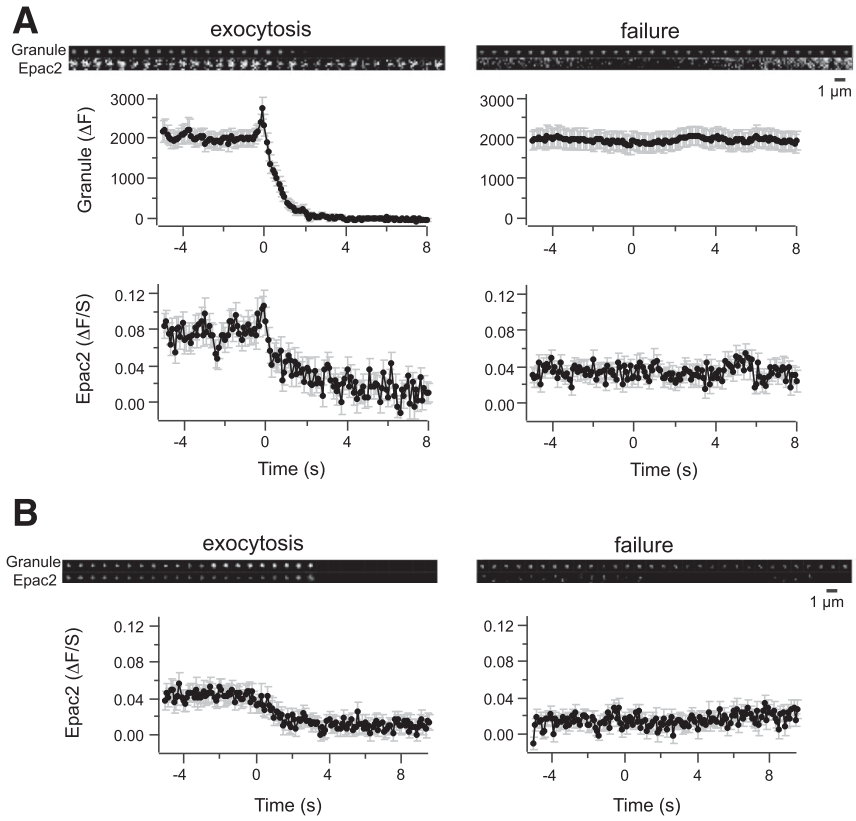

Figure 7—Binding of Epac2A to granule docking sites promotes exocytosis. *A*: TIRF images and intensity recordings (means ± SE) of NPY-GFP (granule) and mCherry-Epac2A-wt in medium containing 10 mmol/L glucose, 200 μmol/L diazoxide, and 2 μmol/L forskolin. Exocytosis was initiated by local application of 75 mmol/L K^+ at time 0. Images were acquired at a rate of 10 s^{-1}. Left panels: Granules undergoing exocytosis show rapid decay of fluorescence and a ΔF/S signal for Epac2 significantly >0 ($P < 0.001$) before the exocytosis event. Right panels: Granules that fail to undergo exocytosis show stable fluorescence and a ΔF/S signal for Epac2 significantly lower than that for exocytosing granules ($P = 0.002$ for averaged period before and $P = 0.03$ for that after time 0). The data represent 52 exocytosis events and 52 failing granules from 9 cells in 3 experiments. *B*: ΔF/S signal for Epac2 in cells stimulated by an increase of the glucose concentration from 3 to 20 mmol/L. The time is aligned to the moment of granule fusion. The data represent 30 events and 30 failing granules from 12 cells in 4 experiments.

targeting mechanism: one that directs the protein to the plasma membrane (the CNB-B and RA domains) and one mediating the specific interaction with the exocytosis machinery (CNB-A domain). We also showed that the localization process regulates granule priming and exocytosis. These findings provide novel insights into the role of cAMP in the regulation of insulin secretion.

Following cAMP binding, Epac2 changes conformation from a closed, autoinhibited state with the N-terminal regulatory region sterically hindering substrate binding at the catalytic site to an open configuration, in which the autoinhibition is relieved (18). This activation results in translocation of the protein from the cytoplasm to the plasma membrane in a cAMP- and Ca^{2+}-dependent manner (10). Previous studies have demonstrated that Epac2 binds to the plasma membrane by interacting with Ras-GTP via the RA domain within its catalytic region (30,31). Accordingly, a point mutation (K684E) in this domain markedly suppresses the activity-dependent Epac2 translocation (Fig. 3) (10). cAMP binding to the second (more COOH-terminal), high-affinity CNB-B domain was also essential to enable membrane interaction (Fig. 3) (10). The role of the

10 μmol/L forskolin (fsk). *D*: TIRF intensity recording in a single α-toxin–permeabilized MIN6 cell coexpressing GFP-Epac1 and mCherry-Epac2A-wt during exposure to increasing concentrations of cAMP. *E*: Means ± SE for the translocation of Epac1 and Epac2 at different cAMP concentrations. The lines are sigmoidal fits of the data. $n = 18$ cells from 5 experiments for both Epac1 and Epac2. *$P < 0.05$ for difference between Epac1 and Epac2. *F*: TIRF images of MIN6 cells coexpressing NPY-mCherry (granule) and GFP-Epac1 under basal conditions (ctrl) and after exposure to 2 μmol/L forskolin (fsk). Scale bar, 2 μm. *G*: Means ± SE for the accumulation of the Epac proteins at granule docking sites quantified as ΔF/S (see RESEARCH DESIGN AND METHODS) under control conditions and after forskolin treatment. Number of cells from at least three experiments is shown for each bar. The values for Epac2 are reproduced from Fig. 4 to enable comparison with Epac1. **$P < 0.01$; ***$P < 0.001$ for difference from control.

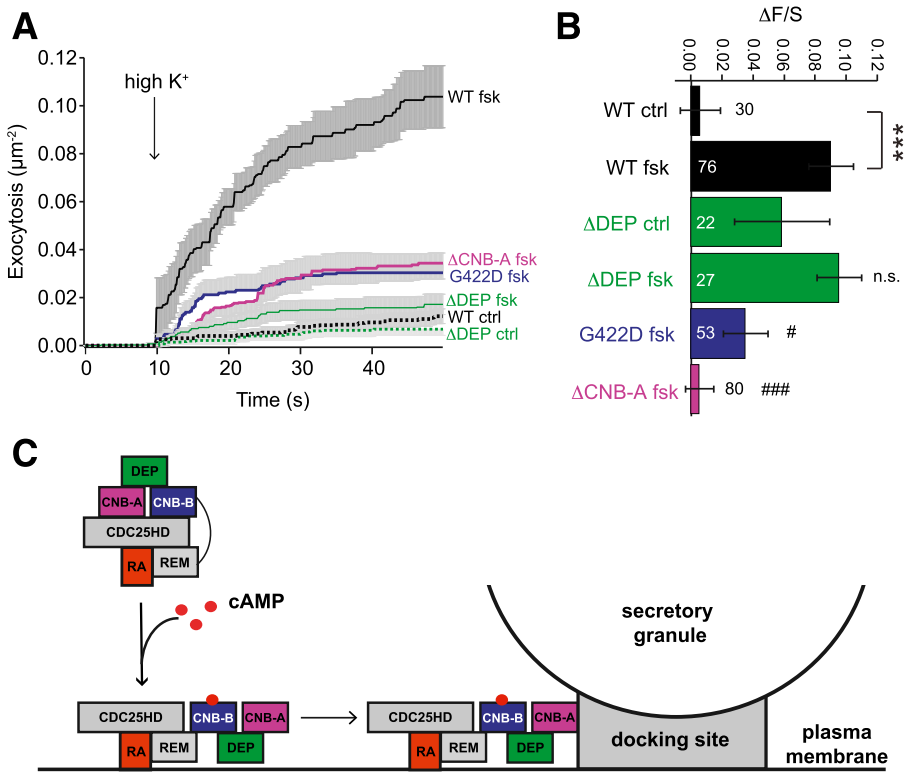

Figure 8—Epac2A localization to the docking sites is necessary, but not sufficient to promote exocytosis. *A*: Means ± SE for the cumulative number of K^+-evoked exocytosis events normalized to cell footprint area in TIRF recordings from MIN6 cells expressing various Epac2A versions in the absence (ctrl) or presence (fsk) of 2 μmol/L forskolin. Compared with wild-type (WT) with forskolin, exocytosis is significantly ($P < 0.001$) impaired in cells expressing the translocation-deficient G422D mutant, in the translocation-competent but granule binding–deficient ΔCNB-A mutant, as well as in the constitutively granule-binding ΔDEP mutant. Data represent 10–13 cells/condition from 2 experiments. *B*: Means ± SE for ΔF/S of the various Epac2A versions at exocytosing granules immediately preceding fusion. The numbers refer to exocytosis events from the same 10–13 cells as in *A*. ***$P < 0.001$; #$P < 0.02$; ###$P < 0.001$ compared to wt with forskolin. *C*: Model for the mechanisms underlying translocation of Epac2A to granule docking sites at the plasma membrane. cAMP binding to the high-affinity CNB-B induces a conformational change of Epac2A. In the activated conformation, the RA domain interacts with the plasma membrane by binding to the small GTPase Ras (not shown). The plasma membrane localization allows the low-affinity CNB-A to interact with proteins associated with vesicle docking sites where Epac2A promotes granule priming and exocytosis.

first (most N-terminal), low-affinity CNB-A domain is less clear, but it has been suggested that it is essential for membrane targeting (11).

In the current study, we investigated the role of the CNB-A and DEP domains using fluorescence-labeled Epac2A mutants and an assay that allows direct comparison of wild-type and mutant protein translocation dynamics in single cells. Experiments with cAMP addition to permeabilized cells showed a left-shifted dose-response relationship for Epac2A translocation after deletion of the CNB-A domain. The deletion potentially increases the accessibility of cAMP to the high-affinity CNB-B domain, because the two domains in the crystal structure occlude each other (14). A similarly improved Epac2A translocation at low to moderate cAMP levels was also observed when cAMP binding to the CNB-A domain was prevented by a single amino acid substitution, probably as a result of increased flexibility of the interface between the two CNB domains (32). The low-affinity domain seemed to contribute to membrane binding only at very high (>30 μmol/L) cAMP concentrations, but it is questionable whether this effect has any physiological relevance, because the translocation response to a high concentration of GLP-1 in intact cells was not reduced by the CNB-A deletion.

DEP domains are typical membrane association domains (33), and in Epac1, the DEP domain is important for cAMP-induced translocation by binding to phosphatidic acid (16). In Epac2, cAMP binding induces significant conformational changes in the DEP domain (32), but its role for Epac2 localization has been unclear. The present data showed that translocation of the DEP deletion mutant was markedly suppressed. Because the assay measures fluorescence intensity changes in relation to the baseline, this effect likely reflects increased Epac2A-ΔDEP association with the membrane under basal conditions rather than a critical role of the DEP domain for membrane binding. This conclusion is supported by the observation of increased membrane localization in confocal images (Fig. 1) and that the mutant protein was present at granule sites irrespective of cAMP (Fig. 4).

The incretin hormone GLP-1 amplifies postprandial glucose-triggered insulin secretion mainly by increasing the β-cell level of cAMP (34), although other mechanisms may also contribute (35). GLP-1 was now found to trigger Epac2A translocation to granule docking sites in both MIN6 cells and primary human islet cells. This effect paralleled the stimulatory action of GLP-1 on cAMP production and was reduced in cells from donors with type 2 diabetes. The latter finding is interesting in light of our recent demonstration that defective cAMP signaling underlies impaired islet function under lipotoxic conditions (27). The domain dependence of the translocation was similar to that for pharmacological increase of intracellular cAMP. These observations indicate that Epac2A translocation to the plasma membrane is required for the physiologically important stimulatory effect of GLP-1 on insulin secretion.

The cAMP-induced translocation of Epac2A to the plasma membrane resulted in clustering of the protein in distinct puncta, which colocalized with secretory granules present at the membrane. There were no signs of association between Epac2A and granules in the cytoplasm as evaluated from confocal images (Fig. 1), and because the membrane binding and granule accumulation processes can be dissociated, we suggest that Epac2A first translocates to the plasma membrane and then becomes associated with the granule docking sites where the protein contributes to the priming process required for vesicle exocytosis (Fig. 8*C*). Although not required for the translocation of Epac2A to the plasma membrane, the CNB-A domain was responsible for this clustering near granules. The granular accumulation did not require cAMP concentrations corresponding to the very high K_d (87 μmol/L) of the CNB-A domain, because it was observed with GLP-1, and this stimulation did not seem to trigger cAMP elevations >30 μmol/L (compare data in Figs. 2 and 3). Moreover, clustering was observed also in response to glucose, which is less efficient than GLP-1 in generating cAMP (36).

The CNB-A domain is only present in the Epac2A splice variant, which is the dominating version in secretory cells, like neurons and β-cells (11). The role of the CNB-A domain for association with the exocytosis machinery is consistent with the localization of the isolated CNB-A domain in clusters at granule docking sites (Fig. 6*A*). Moreover, Epac1, which lacks the CNB-A domain, did not exhibit such clustering, although the protein readily translocated to the plasma membrane in response to cAMP (Fig. 6). Interestingly, the dose dependence of cAMP-induced translocation for Epac1 was more similar to the ΔCNB-A mutant than to wild-type Epac2A. Further studies are warranted to clarify the differential roles of Epac1 and Epac2 at the plasma membrane.

We suggest that the priming process, by which the vesicles are prepared for exocytosis, is regulated by cAMP-dependent clustering of Epac2A to the granule docking sites. Although the levels of endogenous Epac2A could not be assessed in the living cells, we found that granules that underwent exocytosis in response to glucose or K^+ depolarization were associated with more fluorescence-labeled Epac2A than granules, which were docked but failed to release. Moreover, expression of Epac2A mutants associated with impaired translocation or granule accumulation reduced the number of exocytosis events. It is not clear how Epac2A promotes priming and exocytosis, but it is probably related to its interaction with RIM2α (37) or other components of the secretory machinery, such as the SUR1 subunit of the K_{ATP} channel (2), the granular sulphonylurea receptor (21), the active zone protein piccolo (38), or SNAP25 (39).

In summary, we studied the spatiotemporal regulation of Epac2A in β-cells and demonstrate that cAMP-elevating stimuli evokes translocation of the protein from the cytoplasm to the plasma membrane with subsequent clustering at the sites of docked secretory granules, where it regulates priming and exocytosis. Membrane localization is achieved independently of conventional lipid-binding protein modules and instead involves the RA domain that tethers Epac2A to the plasma membrane allowing the CNB-A domain to interact with the exocytosis machinery. Pharmacological stimulation of the processes that localize Epac2A to the vesicles may provide a new strategy for improving insulin secretion in type 2 diabetes.

Funding. This study was supported by grants from the Diabetes Research and Wellness Foundation, the European Foundation for the Study of Diabetes (EFSD-MSD), the Stiftelsen Familjen Ernfors Fond, Novo Nordisk Foundation, the Swedish Diabetes Foundation, and the Swedish Research Council. N.R.G. was supported by the EFSD/Lilly European Diabetes Research Programme and the Swedish Society for Medical Research. Human islets were obtained from the Nordic Network for Clinical Islet Transplantation supported by grants from the JDRF and the strategic grant consortium Excellence of Diabetes Research in Sweden (EXODIAB).

Duality of Interest. No potential conflicts of interest relevant to this article were reported.

Author Contributions. I.A. performed and analyzed Epac2 membrane-binding experiments. N.R.G. performed and analyzed granule imaging and exocytosis experiments. S.B. designed experiments, analyzed data, and edited the manuscript. A.T. conceived the study, designed experiments, analyzed data, and wrote the manuscript. I.A., N.R.G., S.B., and A.T. edited and approved the final version of the manuscript. A.T. is the guarantor of this work and, as such, had full access to all of the data in the study and takes responsibility for the integrity of the data and the accuracy of the data analysis.

Prior Presentation. Parts of this study were presented in abstract form at the 51st annual meeting of the European Association for the Study of Diabetes, Stockholm, Sweden, 14–18 September 2015.

References

1. Gloerich M, Bos JL. Epac: defining a new mechanism for cAMP action. Annu Rev Pharmacol Toxicol 2010;50:355–375

2. Ozaki N, Shibasaki T, Kashima Y, et al. cAMP-GEFII is a direct target of cAMP in regulated exocytosis. Nat Cell Biol 2000;2:805–811

3. Sakaba T, Neher E. Direct modulation of synaptic vesicle priming by GABA(B) receptor activation at a glutamatergic synapse. Nature 2003;424:775–778

4. Shibasaki T, Takahashi H, Miki T, et al. Essential role of Epac2/Rap1 signaling in regulation of insulin granule dynamics by cAMP. Proc Natl Acad Sci U S A 2007; 104:19333–19338

5. Schmidt M, Evellin S, Weernink PA, et al. A new phospholipase-C-calcium signalling pathway mediated by cyclic AMP and a Rap GTPase. Nat Cell Biol 2001;3: 1020–1024

6. Seino S, Shibasaki T. PKA-dependent and PKA-independent pathways for cAMP-regulated exocytosis. Physiol Rev 2005;85:1303–1342
7. Schmidt M, Dekker FJ, Maarsingh H. Exchange protein directly activated by cAMP (epac): a multidomain cAMP mediator in the regulation of diverse biological functions. Pharmacol Rev 2013;65:670–709
8. Ponsioen B, Gloerich M, Ritsma L, Rehmann H, Bos JL, Jalink K. Direct spatial control of Epac1 by cyclic AMP. Mol Cell Biol 2009;29:2521–2531
9. Gloerich M, Ponsioen B, Vliem MJ, et al. Spatial regulation of cyclic AMP-Epac1 signaling in cell adhesion by ERM proteins. Mol Cell Biol 2010;30:5421–5431
10. Idevall-Hagren O, Jakobsson I, Xu Y, Tengholm A. Spatial control of Epac2 activity by cAMP and Ca^{2+}-mediated activation of Ras in pancreatic β cells. Sci Signal 2013;6:1–11, S1–S6
11. Niimura M, Miki T, Shibasaki T, Fujimoto W, Iwanaga T, Seino S. Critical role of the N-terminal cyclic AMP-binding domain of Epac2 in its subcellular localization and function. J Cell Physiol 2009;219:652–658
12. Kawasaki H, Springett GM, Mochizuki N, et al. A family of cAMP-binding proteins that directly activate Rap1. Science 1998;282:2275–2279
13. Høivik EA, Witsoe SL, Bergheim IR, et al. DNA methylation of alternative promoters directs tissue specific expression of Epac2 isoforms. PLoS One 2013;8: e67925
14. Rehmann H, Das J, Knipscheer P, Wittinghofer A, Bos JL. Structure of the cyclic-AMP-responsive exchange factor Epac2 in its auto-inhibited state. Nature 2006;439:625–628
15. de Rooij J, Rehmann H, van Triest M, Cool RH, Wittinghofer A, Bos JL. Mechanism of regulation of the Epac family of cAMP-dependent RapGEFs. J Biol Chem 2000;275:20829–20836
16. Consonni SV, Gloerich M, Spanjaard E, Bos JL. cAMP regulates DEP domain-mediated binding of the guanine nucleotide exchange factor Epac1 to phosphatidic acid at the plasma membrane. Proc Natl Acad Sci U S A 2012;109:3814–3819
17. de Rooij J, Zwartkruis FJ, Verheijen MH, et al. Epac is a Rap1 guanine-nucleotide-exchange factor directly activated by cyclic AMP. Nature 1998;396:474–477
18. Rehmann H, Arias-Palomo E, Hadders MA, Schwede F, Llorca O, Bos JL. Structure of Epac2 in complex with a cyclic AMP analogue and RAP1B. Nature 2008; 455:124–127
19. Rehmann H, Prakash B, Wolf E, et al. Structure and regulation of the cAMP-binding domains of Epac2. Nat Struct Biol 2003;10:26–32
20. Dzhura I, Chepurny OG, Leech CA, et al. Phospholipase C-ε links Epac2 activation to the potentiation of glucose-stimulated insulin secretion from mouse islets of Langerhans. Islets 2011;3:121–128
21. Eliasson L, Ma X, Renström E, et al. SUR1 regulates PKA-independent cAMP-induced granule priming in mouse pancreatic B-cells. J Gen Physiol 2003;121:181–197
22. Henquin JC, Nenquin M. Activators of PKA and Epac distinctly influence insulin secretion and cytosolic Ca^{2+} in female mouse islets stimulated by glucose and tolbutamide. Endocrinology 2014;155:3274–3287
23. Tengholm A, Gylfe E. Oscillatory control of insulin secretion. Mol Cell Endocrinol 2009;297:58–72
24. Gandasi NR, Vestö K, Helou M, Yin P, Saras J, Barg S. Survey of Red Fluorescence Proteins as Markers for Secretory Granule Exocytosis. PLoS One 2015;10: e0127801
25. Dyachok O, Isakov Y, Sågetorp J, Tengholm A. Oscillations of cyclic AMP in hormone-stimulated insulin-secreting β-cells. Nature 2006;439:349–352
26. Miyazaki J, Araki K, Yamato E, et al. Establishment of a pancreatic β cell line that retains glucose-inducible insulin secretion: special reference to expression of glucose transporter isoforms. Endocrinology 1990;127:126–132
27. Tian G, Sol ER, Xu Y, Shuai H, Tengholm A. Impaired cAMP generation contributes to defective glucose-stimulated insulin secretion after long-term exposure to palmitate. Diabetes 2015;64:904–915
28. Gandasi NR, Barg S. Contact-induced clustering of syntaxin and munc18 docks secretory granules at the exocytosis site. Nat Commun 2014;5:3914
29. Barg S, Knowles MK, Chen X, Midorikawa M, Almers W. Syntaxin clusters assemble reversibly at sites of secretory granules in live cells. Proc Natl Acad Sci U S A 2010;107:20804–20809
30. Liu C, Takahashi M, Li Y, et al. Ras is required for the cyclic AMP-dependent activation of Rap1 via Epac2. Mol Cell Biol 2008;28:7109–7125
31. Li Y, Asuri S, Rebhun JF, Castro AF, Paranavitana NC, Quilliam LA. The RAP1 guanine nucleotide exchange factor Epac2 couples cyclic AMP and Ras signals at the plasma membrane. J Biol Chem 2006;281:2506–2514
32. Li S, Tsalkova T, White MA, et al. Mechanism of intracellular cAMP sensor Epac2 activation: cAMP-induced conformational changes identified by amide hydrogen/deuterium exchange mass spectrometry (DXMS). J Biol Chem 2011;286: 17889–17897
33. Consonni SV, Maurice MM, Bos JL. DEP domains: structurally similar but functionally different. Nat Rev Mol Cell Biol 2014;15:357–362
34. Campbell JE, Drucker DJ. Pharmacology, physiology, and mechanisms of incretin hormone action. Cell Metab 2013;17:819–837
35. Shigeto M, Ramracheya R, Tarasov AI, et al. GLP-1 stimulates insulin secretion by PKC-dependent TRPM4 and TRPM5 activation. J Clin Invest 2015;125:4714–4728
36. Tian G, Sandler S, Gylfe E, Tengholm A. Glucose- and hormone-induced cAMP oscillations in α- and β-cells within intact pancreatic islets. Diabetes 2011;60:1535–1543
37. Yasuda T, Shibasaki T, Minami K, et al. Rim2alpha determines docking and priming states in insulin granule exocytosis. Cell Metab 2010;12:117–129
38. Shibasaki T, Sunaga Y, Fujimoto K, Kashima Y, Seino S. Interaction of ATP sensor, cAMP sensor, Ca^{2+} sensor, and voltage-dependent Ca^{2+} channel in insulin granule exocytosis. J Biol Chem 2004;279:7956–7961
39. Vikman J, Svensson H, Huang YC, et al. Truncation of SNAP-25 reduces the stimulatory action of cAMP on rapid exocytosis in insulin-secreting cells. Am J Physiol Endocrinol Metab 2009;297:E452–E461